4328 *Macromolecules* **2009**, *42*, 4328–4336
DOI: 10.1021/ma900394n

Macromolecules
ARTICLE

Deformation-Induced Mobility in Polymer Glasses during Multistep Creep Experiments and Simulations

Hau-Nan Lee,[†,§] Robert A. Riggleman,[‡,§] Juan J. de Pablo,[‡] and M. D. Ediger*[,†]

[†]*Department of Chemistry and* [‡]*Department of Chemical and Biological Engineering, University of Wisconsin-Madison, Madison, Wisconsin 53706.* [§] *The first two authors contributed equally to this work*

Received February 19, 2009; Revised Manuscript Received April 30, 2009

ABSTRACT: Optical photobleaching experiments and molecular dynamics computer simulations were used to investigate changes in segmental mobility during tensile creep deformation of polymer glasses. Experiments were performed on lightly cross-linked PMMA, and the simulations utilized a coarse-grained model. For both single-step and multistep creep deformations, the experiments and simulations show remarkably similar trends, with changes of mobility during deformation exceeding a factor of 100. Both experiment and simulation show a strong correlation between strain rate and mobility in single-step creep. However, in multistep creep, the correlation between strain rate and mobility is broken in both experiment and simulation; this emphasizes that no simple mechanical variable is likely to exhibit a simple relationship with molecular mobility universally. Both simulations and experiments show many features that are inconsistent with the Eyring model.

Introduction

A fundamental understanding of the deformation behavior of polymer glasses is a significant scientific challenge and an active area of research.[1−15] Deformation of polymer glasses is often described as " flow",[1] yet segmental motion in a glass is so slow that liquidlike "flow" is impossible in the absence of deformation. How molecular mobility in polymer glasses is altered by deformation has been considered to be the key to understanding the mechanism of deformation.[12−15] Establishing the connection between molecular mobility and macroscopic deformation could facilitate the development of a predictive model for the deformation of polymer glasses. This would be of great technological significance, for example, in the aerospace industry where polymer composites play an increasingly important role and are expected to support large stresses in a predictable manner for decades.[16]

In previous work, we used an optical photobleaching experiment[17−19] and molecular dynamics (MD) simulations[20,21] to determine the change in the segmental mobility of polymer glasses during uniaxial creep deformation quantitatively. We observed a strong correlation between mobility and strain rate during single-step creep. This correlation is consistent with theoretical work by Chen and Schweizer[22] and has been inferred from purely mechanical measurements.[23] This observation can be interpreted to indicate that stress induces mobility, which in turn allows polymer glasses to flow. Recent experiments[17−19,24,25] and simulations[20,21,26−30] suggest that the external stress can accelerate segmental motion by several orders of magnitude. This result is qualitatively consistent with the phenomenological model proposed by Eyring in 1936[12] and later theoretical work built on the concept of stress-induced mobility.[13−15]

The existence of a simple relationship between microscopic molecular motion and the macroscopic strain rate is striking and would be useful for predicting the deformation behavior of polymer glasses. However, it may not be possible to generalize results from single-step creep measurement to other modes of deformation. Experiments involving different deformations, such as multistep creep or constant strain-rate deformation, are required to test whether this relationship has general validity.

In the present study, we use both experiment and simulation to investigate the relationship between mobility and strain rate during multistep creep deformation of polymer glasses. We use optical photobleaching to measure dye reorientation in lightly cross-linked PMMA during deformation at temperatures between T_g − 19 K and T_g − 9 K. This photobleaching method has been shown to be a reliable method to measure changes in segmental dynamics of polymer glasses under deformation.[17−19] We have also performed MD computer simulations on a coarse-grained model of a polymer glass. Simulations, in addition to allowing the calculation of the quantities measured in the experiment, allow a direct investigation of deformation-induced changes in molecular structure, the underlying potential energy landscape, and many other features that are not directly accessible by experiment.[20,21,31] A direct comparison of experimental and computational results allows us to understand the role of the probe molecules in the experiments, test the validity of the simulation model, and ultimately provide a molecular interpretation of the experimental observations.[20,21,31]

We find that for both single-step and multistep creep deformations the experiments and simulations show remarkably similar trends, with changes of mobility during deformation exceeding a factor of 100. The strong correlation between strain rate and mobility is only exhibited in single-step creep deformation. In multistep creep and recovery, the correlation between strain rate and mobility is broken, emphasizing that no simple mechanical variable universally exhibits a simple relationship with molecular mobility. Both simulations and experiments show many features that are inconsistent with a simple application of the Eyring model. For example, after reducing the stress, the mobility decreases more than an order of magnitude, whereas the true stress is constant. In addition, we observe that after flow onset the dynamics become more homogeneous, as evidenced by an increase in the KWW β parameter observed in the experiment.

*To whom correspondence should be addressed. E-mail: ediger@chem.wisc.edu.

 Published on Web 05/29/2009

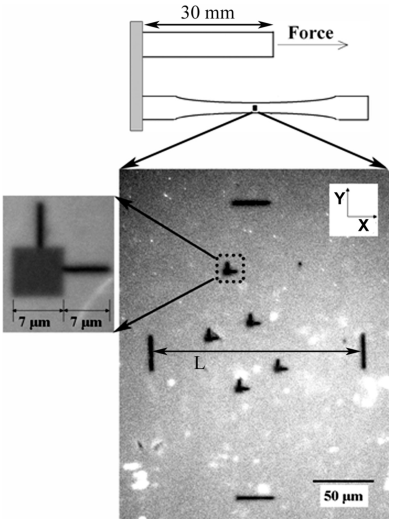

Figure 1. Experimental geometry for local measurements of strain and mobility. The four photobleached lines define the region where local strain and mobility measurements are performed. The change in the distance along the X direction between the photobleached lines defines the local strain, $\varepsilon(t) = (L(t) - L_0)/L_0$. The small patterns are used for measurements of dye reorientation; one of these is shown in detail on the left.

Experimental Methods

Sample. The sample preparation procedure has been previously described.[17] Lightly cross-linked poly(methyl methacrylate) (PMMA) containing 10^{-6} M probe molecules (DPPC; *N*, *N*′-dipentyl-3,4,9,10-perylenedicarboximide) was prepared using thermally initiated radical polymerization. The dimensions of the PMMA film utilized for experiments are 2.5 × 30 mm, and the thickness is 25 μm. The onset value for the glass transition temperature (T_g) for the PMMA samples is 395 K, as determined by differential scanning calorimetry obtained from the second heating scan at 10 K/min.

Local Creep Measurement. A temperature-controlled deformation cell was used for local creep and mobility measurements.[17] Deformation of the PMMA film was achieved by uniaxial tensile creep. The sample was subjected to a constant engineering stress, $\sigma_0 = F/A_0$, where F is the applied force and A_0 is the original cross-sectional area of the sample. The true stress increases as deformation continues and is defined as the ratio of the applied force (F) to the instantaneous cross-sectional area (A). Figure 1 illustrates some features of the local measurements of strain and DPPC reorientation. Local strain and mobility were measured optically in the same small region of the sample.[17,18] We photobleached four lines in the center of the sample, defining the region (~200 × 250 μm^2) of measurements. A CCD camera was used to photograph this small region at many time points during the creep experiment. The local strain is defined as the increase in distance between the two photobleached lines ($L(t)$) perpendicular to the direction of deformation (x axis), $\varepsilon(t) = (L(t) - L_0)/L_0$. Dye reorientation measurements were performed inside the region defined by these four lines as described below. This local strain measurement allows us to determine unambiguously the strain in the region where the mobility measurements are performed. Because L_0 is only about 200 μm and no distortion of the photobleached lines was observed during deformation, we can safely assume that the sample deforms homogenously in this small region.

Prior to each deformation measurement, the sample was heated to 405 K in the absence of stress for at least 3 h to erase the thermal and mechanical history. The sample was then cooled to the testing temperature at 1 K/min and aged for 30 min prior to the initiation of the creep experiment.

Dye Reorientation Measurement. Photobleaching measurements of dye reorientation have been previously described.[17,32] We use a confocal fluorescence microscope system to measure the reorientation of DPPC probe molecules in PMMA glasses. The reorientation of this dye molecule is strongly correlated with the segmental dynamics of PMMA, as shown in previous studies.[17−19] Multiple measurements of dye reorientation can be made during one creep experiment to define the mobility change as a function of time.

In the experiments reported here, we used an intense linearly polarized laser beam (532 nm) to photobleach probe molecules. The probe molecules with absorption dipoles aligned with the polarization of the light are selectively photobleached. This creates an orientationally anisotropic distribution of unbleached dye molecules in the sample. With time, the unbleached probes reorient, regenerating an isotropic distribution. To monitor this process, a weak circularly polarized reading beam is introduced to illuminate the bleached area immediately after photobleaching. The fluorescence induced by the reading beam is separated into parallel and perpendicular components, and the time-dependent anisotropy decay, $r(t)$, is defined by the following equations[17]

$$r(t) = \frac{\Delta I_{//}(t) - \Delta I_{\perp}(t)}{\Delta I_{//}(t) + 2\Delta I_{\perp}(t)} \tag{1}$$

$$\Delta I_{//}(t) = I_{//}^{\mathrm{un}}(t) - I_{//}(t) \tag{2}$$

$$\Delta I_{\perp}(t) = g \cdot I_{\perp}^{\mathrm{un}}(t) - g \cdot I_{\perp}(t) \tag{3}$$

Here $\Delta I_{//}(t)$ is the difference in the parallel fluorescence intensity between an unbleached part of the sample and the bleached part of the sample at time, t, after bleaching; $\Delta I_{\perp}(t)$ is defined analogously. The correction factor, g, is used to correct for the dye alignment, the efficiencies of the two detectors, and the imperfection of the circularly polarized reading beam.[17]

The $r(t)$ measured with the photobleaching technique is proportional to the second-order orientation autocorrelation function CF(t) of the absorption dipole, $\hat{\mu}$, for the DPPC molecule: $\mathrm{CF}(t) = r(t)/r(0) = \langle P_2[\hat{\mu}(0)\cdot\hat{\mu}(t)]\rangle$, where P_2 is the second Legendre polynomial. We fit the anisotropy decays with the stretched exponential function (KWW function), $\mathrm{CF}(t) = e^{-(t/\tau)^{\beta}}$, and define the rotational correlation time, τ_c, as the integral of the correlation function.

The error in log τ_c is determined by how much anisotropy decay we observe in a mobility measurement (~340 s duration). During the creep experiments shown in this study, we always observe more than 50% of the anisotropy decay, and fits to KWW function provide us with reliable results. The error in log τ_c is typically ±0.1 for these measurements. However, for an undeformed sample, the reorientation of dye molecules is so slow that we only observe a small portion (~35%) of the anisotropy decay in each mobility measurement (~340 s). Under these conditions, we cannot accurately determine the KWW β parameter and, as a result, there is a large error in the τ_c. Therefore, the rotational correlation time for the undeformed sample ($\tau_{c,\mathrm{undeformed}}$) is obtained by fitting the anisotropy decay curves to the KWW function by keeping β fixed at 0.32. The choice of $\beta = 0.32$ as a constraint is based on two observations. First, the average value of β for DPPC rotation in PMMA near T_g in the absence of deformation is 0.32 ± 0.02. Second, we fit 27 slow anisotropy decay functions obtained at 375.7 K (low strain experiments, before the onset of flow) with the unconstrained KWW function. The average value of β for these data is 0.31 ± 0.03. Because of the relatively small decay of the anisotropy function, the error in log τ_c is typically ± 0.2 for an undeformed sample. A detailed discussion of data analysis procedure and error estimation can be found in a previous study.[19]

During each anisotropy decay measurement (~340 s duration), the mobility of the polymer glass evolves continuously. In this circumstance, the mobility that we report is an average mobility over this time interval because the rotational correlation time is calculated by integrating the normalized anisotropy decay. For measurements immediately after loading or unloading stress, significant changes in mobility may occur during the acquisition of an anisotropy decay curve. Whereas this has little impact on the mobility that we report, it could result in a larger error in the fitted value of the KWW β parameter for this interval.

For each mobility measurement, we photobleached a $7 \times 7\ \mu m^2$ square pattern (Figure 1, left) on the sample.[17] The time-dependent anisotropy decay is measured in the center of the square. During creep, this photobleached pattern moves along the direction of deformation. To track the pattern, a piezo positioner is used to drive the sample in the opposite direction of the deformation.

Simulation Methods

Molecular Model. The polymer model used in this work consists of 81 chains with 500 Lennard-Jones (LJ) interaction sites on each chain in a simulation box with periodic boundary conditions. Neighboring sites on the polymer backbone are connected with very stiff harmonic bonds, and all nonbonded interactions are taken into account with an LJ interaction potential that is cutoff at a distance of $r = 2.5\sigma$, where σ is the size of a polymer monomer. For complete details of the model, we refer the reader to refs 21 and 33. The LJ potential is shifted such that the energy and forces both go smoothly to zero at the cutoff. All units for the simulation results, denoted with *, are reduced by the LJ parameters of the polymer monomers σ, ε, and mass, m (i.e., $T^* = kT/\varepsilon$, $P^* = P\sigma^3/\varepsilon$, $t^* = t(m\sigma^2/\varepsilon)^{1/2}$).

At the chain length considered here, each chain contains approximately eight entanglements,[34] and the extremely long relaxation times associated with such polymers render equilibration using traditional MD difficult. We therefore employ Monte Carlo (MC) techniques at a high temperature to ensure proper relaxation of our polymer chains. Our MC moves include connectivity-altering, configurational bias double-rebridging moves that enable very efficient relaxation of the end-to-end autocorrelation function.[35] After generating three independent equilibrated samples using MC at $T^* = 1.2$, our materials were cooled at a rate of $\Delta T^*/\delta t = 10^{-4}$ to $T^* = 0.35$ at $P^* = 0.3$ using MD in the NPT ensemble. The glass transition temperature is $T_g^* = 0.373 \pm 0.001$ at this cooling rate, which is estimated by identifying the break in the density versus temperature curve. All uncertainties are determined from the standard error among the three independent configurations.

After cooling to $T^* = 0.35$, all samples were aged for $t^* = 10\,000$ in the NPT ensemble. We performed creep deformations by imparting constant true tensile stresses in the x direction while maintaining a constant pressure of $P^* = 0.3$ in the y and z directions. We measure the strain by monitoring the change in the x dimension of our simulation box as a function of time. Consistent with the experiments reported here, the strain is defined as $\varepsilon(t) = (Lx(t) - Lx_0)/Lx_0$.

Bond Autocorrelation Function. We measure the segmental dynamics during deformation using the bond autocorrelation function, $C_b(t)$, defined as $C_b(t) = \langle P_2(\mathbf{b}_i(t)\cdot\mathbf{b}_i(0))\rangle$. Here $P_2(x)$ is the second Legendre polynomial, $\mathbf{b}_i(t)$ is a unit vector aligned along the i^{th} bond on the polymer backbone at time, t, and the angular brackets indicate an average over both of the bonds in our sample and time origins. Similar to our previous work,[20,21] we calculate $C_b(t)$ in time windows of size $t^* = 1000$; that is, for a given deformation simulation, we obtain several measurements of $C_b(t)$, each of which yield a relaxation time. When we average over time origins, all of the time origins are restricted to the time window of interest. Similar to the experimental approach, we fit each $C_b(t)$ to the KWW stretched exponential and obtain an effective relaxation time as $\tau_b = a_0\cdot\tau_0\cdot\Gamma(1/\beta)/\beta$. We employ a pre-exponential factor, a_0, in the KWW expression because $C_b(t)$ decays by approximately 5% on time scales shorter than our sampling time; this initial decay corresponds to dynamics associated with the ballistic regime and is not relevant to the α process. Previous studies[36] have shown that relaxation times obtained from $C_b(t)$ are indicative of the α relaxation time in glass-forming polymers in the supercooled regime where the α relaxation time is readily accessible with MD simulations. We measure τ_b for the undeformed material by performing a long MD simulation beginning after the aging step of our sample preparation. The undeformed τ_b is estimated to be $18\,0000 \pm 60\,000$.

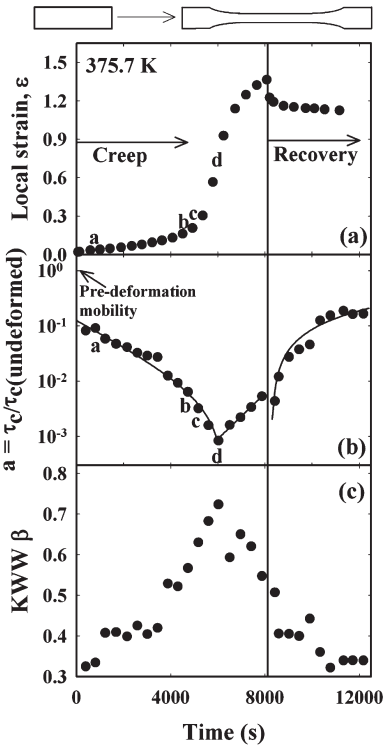

Figure 2. (a) Creep experiments on PMMA at 375.7 K with an engineering stress of 16.0 MPa, followed by recovery with an engineering stress of 0.7 MPa. The initial and final shapes of the sample are shown. The labels a−d refer to Figure 3. (b) Mobility shift factor during creep and recovery. The mobility increases more than 1000 times relative to the undeformed state. The solid lines are guides to the eye. (c) KWW β parameter during creep and recovery.

Experimental Results

Change in Mobility during a Single-Step Creep Experiment. Figure 2 shows the evolution of the strain and the segmental mobility for PMMA glass during creep deformation at 375.7 K (T_g − 19 K) with engineering stress of 16.0 MPa. Data for subsequent recovery at very low stress is also shown. Panel a shows the local strain as a function of time during creep and recovery. When subjected to this large stress, the sample underwent flow and strain hardening. Up to $\varepsilon = 0.15$, the sample deformed homogeneously, after which necking occurred. In this experiment, the strain rate continuously increased after the stress was applied, indicating that the sample began flow essentially immediately. After ~6000 s (the inflection point of

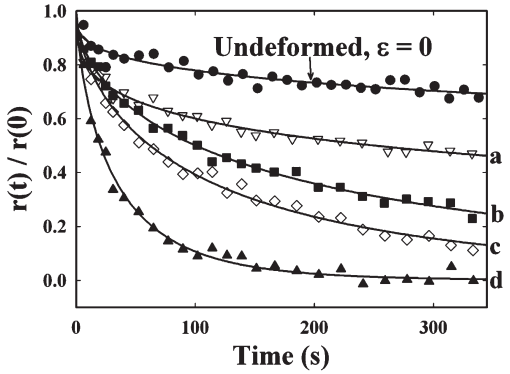

Figure 3. Normalized anisotropy decays obtained during the creep experiment at 375.7 K with engineering stress of 16.0 MPa at times indicated by letters a−d in Figure 2. As the strain rate increases, higher mobility (faster anisotropy decay) is observed. The solid lines are KWW fits to the data.

the strain curve), the strain rate decreased because of strain hardening. After lowering the stress to ~0.7 MPa, the strain slowly and partially recovered.

We performed ~30 photobleaching experiments during creep and recovery to measure the segmental mobility of the PMMA glass in different stages of deformation. Some anisotropy decays measured in the flow regime during creep at 375.7 K are illustrated in Figure 3. The data clearly show that the anisotropy functions decay faster as the strain and strain rate increase (curves a−d), indicating that mobility increases during this stage of the deformation.

To analyze the changes in segmental mobility during creep and recovery quantitatively, we fit the anisotropy decays to the KWW equation and obtain the rotational correlation time, τ_c. We define the mobility shift factor $a = \tau_{c,deformed}/\tau_{c,undeformed}$, and this quantity is shown in Figure 2b. Immediately after the stress is applied, the mobility increases by a factor of 10. As the strain rate increases, the mobility continually increases until dynamics are accelerated more than 1000-fold relative to the undeformed glass. In single-step creep experiments, the highest mobility enhancement always occurs at the time with the highest strain rate. As the sample enters the strain hardening regime ($\varepsilon \approx 0.7$), the mobility decreases as the strain rate decreases, even though the strain and true stress continually increase.

Figure 2c shows the KWW β parameter, as obtained by fitting the anisotropy decays, in different stages of the deformation. Initially, the KWW β parameter continually increases as mobility and strain rate increase. In the strain-hardening regime, the KWW β decreases as mobility and strain rate decrease. During recovery, the KWW β parameter further decreases toward the undeformed value (0.32) as the mobility decreases.

Figure 4 shows data for a creep and recovery experiment at 385.7 K (T_g − 9 K) with engineering stress of 9.0 MPa. The qualitative features of Figure 4 are identical to those displayed in Figure 2. As is well known,[1,23] flow occurs at lower stress levels as T_g is approached from below. At both temperatures, we also performed experiments at somewhat lower stress levels (data not shown here, see ref 19). Under these conditions, the strain rate first decreases, passes through a minimum, and then continuously increases as the sample flows. In such experiments, we define flow onset as this minimum in the local strain rate.

We draw attention to two features in Figures 2 and 4. First, the data at both temperatures exhibit a strong correlation among the KWW β parameter, the strain rate, and the mobility. The highest mobility enhancement always comes with the largest strain rate and KWW β value. As we show below, these correlations do not persist in multistep creep experiments. Second, at both temperatures, after removing the stress, the mobility surprisingly first increases and then decreases toward the mobility of the undeformed PMMA. This observation is

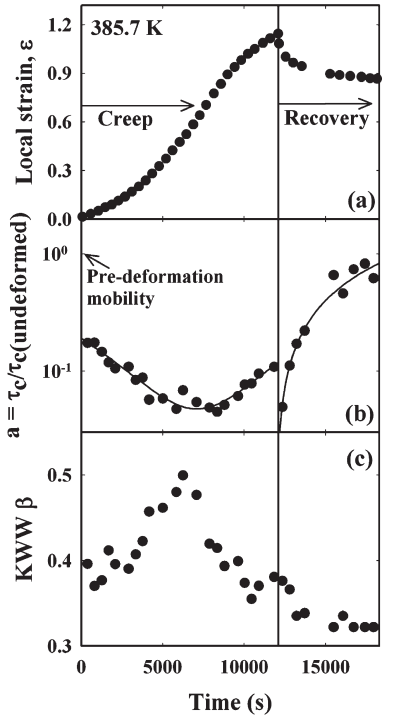

Figure 4. (a) Creep and recovery experiments on PMMA at 385.7 K with an engineering stress of 9.0 MPa. (b) Mobility shift factor during creep and recovery. The solid lines are guides to the eye. (c) KWW β parameter during creep and recovery.

consistent with recent experiments[18,19] and with the simulation results described below.

Change in Mobility during a Multistep Creep Experiment. Figure 5 illustrates segmental mobility measurements during multistep creep experiments on PMMA at 375.7 K. Panels a and b show the imposed stress profile and the resulting local strain response. This deformation scheme was utilized by Kramer to study "stress aging" in polymer glasses.[37] Deformation started with a constant engineering stress of 15.0 MPa (step A). In this step, the local strain continually increases up to 0.5. The engineering stress was then reduced to 6.0 MPa for 1 h (step B). During this time, the strain rate was nearly constant at a very small value. Next, the engineering stress of 15.0 MPa was again applied (step C), and the local strain increased at a constant strain rate. Finally, the stress was removed and the strain partially recovered (step D).

Panels c and d shows the time evolution of the mobility shift factor and the KWW β parameter during multistep creep. In step A, these observables respond as in the single-step creep measurements shown in Figures 2 and 4. After the engineering stress was lowered to 6.0 MPa (step B), both the mobility and KWW β drop significantly, and the mobility slowly decreases. We emphasize that whereas the true stress and strain rate are essentially constant in this step, the mobility changes considerably. In step C, immediately after the engineering stress was returned to 15.0 MPa, the mobility increased significantly. However, the mobility is smaller than the mobility during the last measurement in step A, even though the true stresses are the same. The mobility then slowly increases, passes through a maximum, and finally decreases because of strain hardening. The KWW β parameter also jumps to high values after the increase in stress. Even though the strain rate is constant in this step, the mobility and the KWW β parameter continually evolve. The change in the mobility and the KWW β in step D are similar to the recovery in the single-step creep experiments in the previous section, except for one feature. In Figure 5c, no increase in mobility is observed immediately after the stress is removed. We believe that this is because the highest strain in the

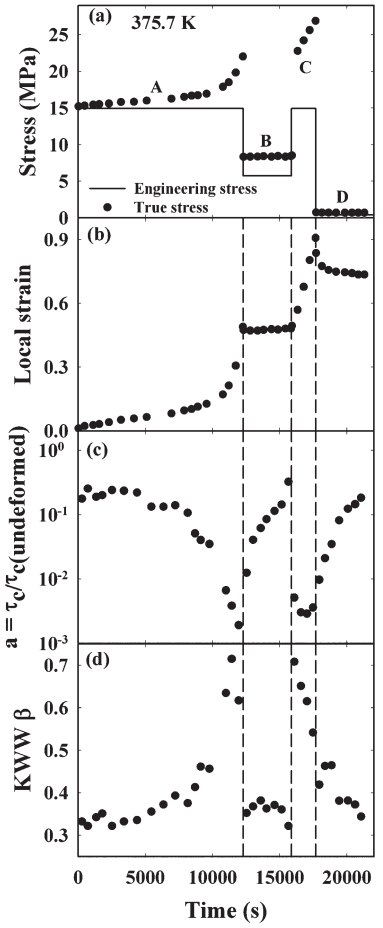

Figure 5. Multistep creep experiment on PMMA at 375.7K. (a) Engineering stress and true stress profile. The labels A−D are utilized in Figures 9a and 10a. (b) Measured local strain. (c) Mobility shift factor. (d) KWW β parameter.

multistep creep was only ~0.9, whereas the strain in the single-step creep was greater than 1.2. In our experiments to date, only samples deformed far into the strain-hardening regime have shown an increase in mobility immediately after the stress is lowered.

Simulation Results

Change in Mobility during a Single-Step Creep Deformation. The strain response for single-step creep deformation at a true stress of 0.62 for the model polymer is shown in Figure 6a. A constant true stress of 0.62 was employed until $t^* = 8000$ when the stress was removed and the material was allowed to recover for an additional $t^* = 4000$. At very short times ($t^* < 20$), there is an elastic response of our sample, followed by a brief period of deformation at nearly constant strain rate ($20 < t^* < 300$). Next, the strain rate increases as the material begins to flow until strain hardening decreases the strain rate for strains larger than 0.25 ($t^* \approx 2000$). This value of strain for the onset of strain hardening is consistent with that reported elsewhere for constant strain rate deformation.[38] In contrast with the experiments (where necking was observed), the deformation in the simulations is completely homogeneous because of the periodic boundary conditions.

Examples of the bond autocorrelation function are plotted in Figure 7 at four different times during the single-step creep. Immediately after the stress is applied, the mobility is significantly enhanced compared with the undeformed sample, as evidenced by the significantly faster decay of $C_b(t)$

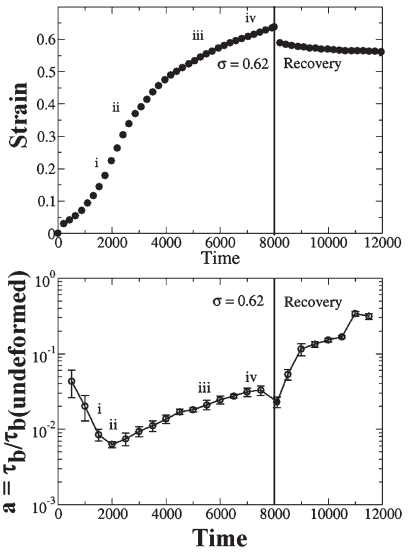

Figure 6. (a) Molecular dynamics simulations of creep and recovery at $T^* = 0.35$ at a constant true stress of 0.62. The small Roman numerals refer to Figure 7. (b) Mobility shift factors during creep and recovery. The mobility at $t^* = 8100$ (just after removing the stress) was measured using a smaller time window than that of the other points. All uncertainties are determined from the standard error among the three independent configurations. The error bar for the shift factor reflects the uncertainty in τ_b (deformed) but does not reflect the uncertainty in the undeformed value of τ_b.

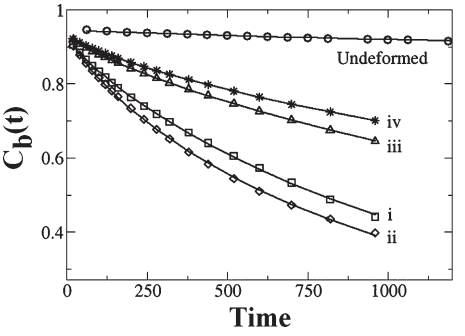

Figure 7. Bond autocorrelation functions obtained during simulations of creep deformation with a true stress of 0.62 at the times indicated by the small Roman numerals in Figure 6. The bond autocorrelation function decays most rapidly during periods of high strain rate. The solid lines are KWW fits to the data.

(curve i). The mobility further increases (curve ii in Figure 7) until strain hardening decreases the strain rate (curves iii and iv).

These effects are quantified in Figure 6b, where we plot the mobility shift factors obtained from our fits of $C_b(t)$ to the KWW stretched exponential. Immediately after the stress is applied, the mobility shift factor decreases by more than an order of magnitude. As flow continues, the mobility increases by another order of magnitude until $t^* = 2000$, where strain hardening begins. Here the strain rate decreases and the mobility also decreases until the stress is removed at $t^* = 8000$. To capture the transient increase in mobility upon removal of the stress, we use a time window that is only $t^* = 200$ (five times smaller than that used otherwise). We find that the mobility is briefly enhanced when the stress is removed. Beyond this point, the mobility gradually decays back toward the undeformed value.

Change in Mobility during a Multistep Creep Deformation. The stress cycle applied during our multistep creep deformations is outlined in Figure 8a. We began with a stress of 0.62

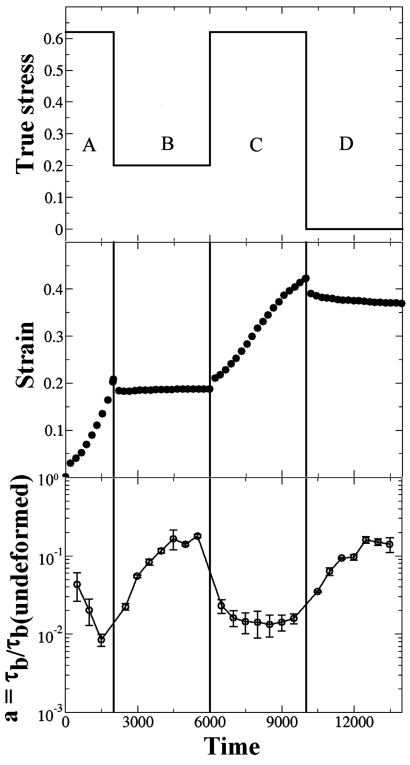

Figure 8. Molecular dynamics simulations of multistep creep at $T^* = 0.35$. (a) True stress profile applied to the sample. The labels A−D are utilized in Figures 9b and 10b. (b) Strain response. (c) Mobility shift factor. All uncertainties are determined from the standard error among the three independent configurations. The error bars do not reflect the uncertainty in the undeformed value of τ_b.

for $t^* = 2000$, then the stress was reduced to 0.2 for $t^* = 4000$, followed by a subsequent increase to 0.62 for $t^* = 4000$ and finally recovery at zero stress for $t^* = 4000$. During the initial step (step A) with a true stress of 0.62 (the same as that employed in Figure 6), the strain response shown in Figure 7b is identical to that shown above up to $t^* = 2000$. This time corresponds to the maximum in the strain rate before strain hardening begins in Figure 6, and in Figure 6b, we see that the mobility monotonically increases until $t^* = 2000$. At this point (step B), the stress is reduced to 0.20, and the polymer exhibited an elastic retraction where the strain decreased. After this initial elastic retraction, the polymer slowly deforms at a very low, nearly constant strain rate; throughout this step, the mobility decreases by approximately an order of magnitude, even though the strain rate is essentially constant. The stress was once again increased at $t^* = 6000$ (step C). The polymer quickly begins to flow, and the mobility immediately increases. We point out that the mobility at the beginning of step C is lower than that at the end of step A, even though the stress is the same. Finally, in step D, the stress is removed and the mobility decreases back toward its undeformed value.

Discussion: Comparison between Experiment and Simulation

As we describe in this section, there is a remarkable similarity between the simulations and experiments with regard to segmental mobility changes during creep deformation.

Single-Step and Multistep Creep. In single-step creep (Figures 2, 4, and 6), experiment and simulation both indicate very large increases (up to a factor of 1000) in segmental mobility during deformation. Both experiment and simulation show that the mobility continually increases during flow until the onset of strain hardening. Moreover, both experiment and simulation show a sudden increase in segmental mobility immediately after the stress is removed.

In multistep creep (Figures 5 and 8), many features of the experiment and simulation are in excellent agreement. In step A, as in the single-step creep, the mobility increases as the sample flows. After the engineering stress is lowered (step B), the mobility first drops significantly and then decreases slowly, even though the strain rate and true stress are essentially constant in this step. In step C, immediately after the stress is reapplied, the mobility increases significantly but is initially smaller than the mobility of the last measurement in step A. Even though the strain rate is essentially constant in this step, the mobility continually evolves. In step D, the mobility slowly decreases toward the undeformed mobility of polymer glass.

One obvious difference between experiment and simulation is that large changes in the KWW β parameter were observed in experiment, whereas no significant change in β was observed in simulation. In principle, this might be due to a number of factors, including the use of a probe molecule in the experiment and a coarse-grained model in the simulation. It is important to note that the KWW β parameter for the undeformed glass is much lower in the experiment (0.32) than in the simulation (0.8). The smaller value of β indicates a broader distribution of relaxation times and likely also indicates a more heterogeneous set of dynamic environments in the glass.[39−41] Because the simulation dynamics are already relatively homogeneous in the absence of deformation, there is little room for homogeneity to increase with deformation, and any changes that do occur are difficult to discern because of the uncertainty in determining β.

The results observed in both experiments and simulations in step C are consistent with the "stress aging" phenomenon reported by Kramer.[37] In his study, a semicrystalline (partially glassy) nylon sample was aged at a stress below the stress initially used to drive the flow in a tensile creep experiment.[37] Upon resumption of the original stress, he reported a "delay time" before steady-state flow was reestablished, which was interpreted as aging of the sample during the period of lower stress.[37] The lower mobility at the beginning of step C (in comparison with the end of step A) is qualitatively consistent with the delay time observed by Kramer.

Mobility As a Function of True Stress. Figure 9a shows experimental measurements of mobility as a function of true stress at 375.7 K. The "×" points show data obtained from single-step creep (Figure 2 and refs 18 and 19), and data from two different types of experiments are included. For all of the points with stress less than 15.0 MPa, we obtained the data by performing a single mobility measurement immediately after applying the stress. In these experiments, the deformations are homogeneous, and the strains are generally very small ($\varepsilon < 0.05$). Results from Figure 2 are also presented; here multiple mobility measurements are performed during one creep experiment, and the overall strain is large ($\varepsilon \approx 1.4$); for these experiments, the mobility is plotted as a function of the instantaneous true stress. Three different regimes are illustrated by the "×" points in Figure 9a.[18] In the low stress regime (< 15 MPa), the Eyring model[12] can reasonably describe the data. The Eyring model predicts that the response of the segmental relaxation time, τ, of a polymer glass to an applied stress, σ, is $\tau \propto \sigma/\sinh[(\sigma \cdot V)/(2 \cdot k_b T)]$, where $k_b T$ is the thermal energy and V is the activation volume. Fitting the low stress data to the Eyring model yields $V = 2.7$ nm.[3] A very large mobility enhancement is observed after the onset of flow ($\sigma > 15$ MPa), and the Eyring model fails to capture this behavior. In the strain hardening regime, large

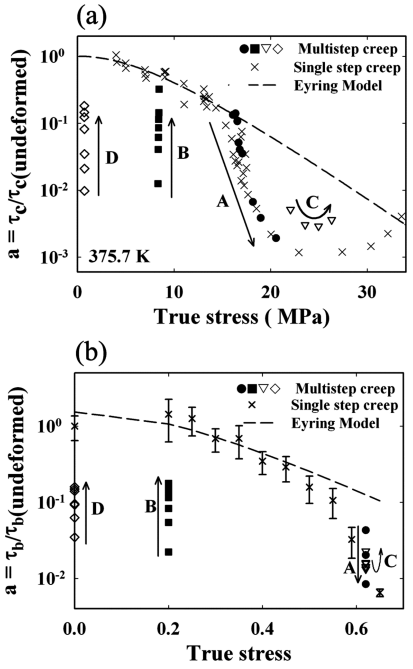

Figure 9. (a) Mobility shift factor as a function of true stress for the multistep creep experiment shown in Figure 5. The "×" points show data obtained from single-step creep (Figure 2 and refs 18 and 19). The multistep creep results do not fall on this curve after period A. The labels A−D refer to Figure 5, and the arrows show the direction of time. The dashed line shows a fit to the Eyring model. (b) Mobility shift factor as a function of true stress from the multistep creep simulations shown in Figure 8. The "×" points indicate data from single-step creep simulations. The labels A−D are defined in Figure 8. The dashed line is a fit to the Eyring model.

strains orient polymer chains, and the resulting structure effectively resists deformation; strain hardening is associated with the upturn of the mobility at large stress.[42] A thorough discussion of the influence of external stress on the molecular mobility of this polymer glass can be found elsewhere.[18,19]

Figure 9b shows the mobility as a function of stress from MD simulations. In these simulations, the true stress is constant during creep deformation. The "×" points represent data obtained from single-step creep. Similar to the low strain experiments described above, in these simulations, we perform a single bond autocorrelation function measurement immediately after applying the stress. For simulations with $\sigma \geq 0.59$, the onset of flow begins in the time window for the first bond autocorrelation function measurement. As in experiment, the Eyring model can describe the data in low stress regime. A reasonable fit is obtained for simulations with stresses below 0.45, although the model overpredicts the zero stress value of τ_b. An activation volume, $V^* = 3.84$, is obtained in good agreement with previous simulations.[21] Consistent with the experimental results, the three simulation points from the flow regime ($\sigma \geq 0.59$) fall significantly beneath the Eyring curve. At $\sigma = 0.65$, the observed mobility is more than 10 times faster than that predicted by the Eyring fit to the low stress data.

In both panels of Figure 9, we have shown results from multistep creep as solid or open symbols. There is an excellent qualitative alignment between simulation and experiment. This is most obvious for the steps B and D. At first glance, steps A and C appear to be rather different in the two panels, but this is explained by the different independent variables in the experiment (engineering stress) and simulation (true stress). In the simulations, the increase in mobility at constant true stress in step A is consistent with the (even larger) increase in mobility in step A of the experiments (which gets spread across a range of true stresses). Similarly, both experiment and simulation show an increase and then a decrease in mobility during step C.

The multistep creep results from both simulation and experiment are strongly inconsistent with a simple application of the Eyring model. An essential feature of the Eyring model is that mobility is a function of the instantaneous stress. Yet both the experiment and simulations show that a wide range of mobilities (up to a factor of 100) can be obtained at a single stress level.

The Eyring model does not consider the fact that a polymer glass is in a nonequilibrium state before, during, and after deformation. In modern terms, the position of the sample on the potential energy landscape is constantly evolving whether or not stress is applied.[11,21,43,44] Qualitatively, this explains two features of our simulations and experiments that are inconsistent with the Eyring model. We have already discussed Figures 5 and 8 in terms of the "stress aging" concept utilized by Kramer. We expect that "aging" (i.e., downward motion on the energy landscape) is always occurring in these samples and that the enhanced mobility that occurs during high stress may lead to faster aging after the stress is lowered. The high mobility observed immediately after the stress is removed (Figures 2, 4, and 6) can also be qualitatively understood in terms of the energy landscape. When the stress is removed, a nearly instantaneous strain recovery occurs. In this process, chain segments quickly rearrange and do not have an opportunity to optimize packing. Therefore, the system is left high on the energy landscape with the high mobility characteristic of inefficient packing.

Correlation between Mobility and Strain Rate. Figure 10a shows experimental measurements of instantaneous strain rate as a function of mobility at 375.7 K. The "×" points show data obtained from single-step creep (Figure 2 and refs 18 and 19). The single-step creep data show a strong correlation between mobility and strain rate, suggesting that under these conditions, mechanical flow occurs at a rate that is controlled by segmental dynamics.[18] Figure 10b shows strain rate as a function of mobility from the MD simulations. The "×" points show data obtained from single-step creep (Figure 5 and ref 38). The single-step creep data from the simulation also show a good correlation between mobility and strain rate, except for the first measurement after applying the stress ("◐" points). In the simulations, the first mobility measurement immediately after the stress is imposed always has slightly lower mobility.

The solid and open symbols in Figure 10 show that multistep creep results from both experiment (data from Figure 5) and simulation (data from Figure 8) do not fall on the master curve, particularly for step B. In both experiment and simulation, reducing the stress makes the strain rate essentially constant in step B, whereas mobility continually decreases for nearly a decade. In steps C and D, the experiments show smaller systematic deviations from the single-step creep master curve. These observations show that the strong correlation between strain rate and mobility during single-step creep is a special case that is not generally observed. It is likely that no simple mechanical variable universally exhibits a simple relationship with molecular mobility.

Experiment/Simulation Synergy. We wish to discuss briefly what can be learned from the combination of experiments and simulations. If only simulations had been performed, then they could be criticized as unrealistic because the polymer model is coarse-grained. Furthermore, the

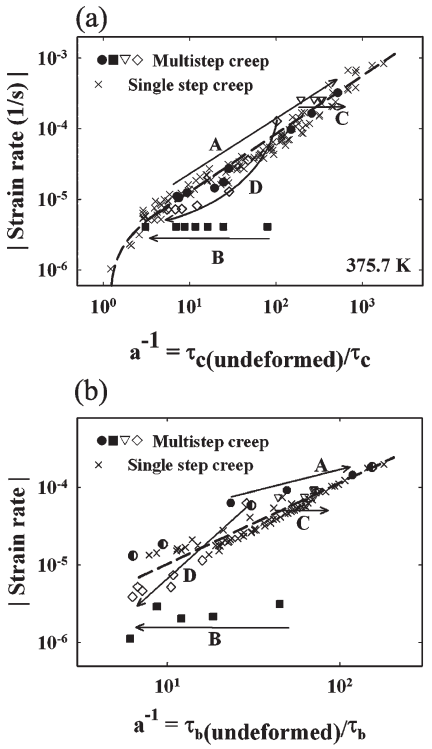

Figure 10. (a) Strain rate as a function of mobility for the multistep creep experiment shown in Figure 5. The "×" points show data obtained from single-step creep (Figure 2 and refs 18 and 19). The single-step creep data show a strong correlation between mobility and strain rate. The dashed line is a guide to the eye. The multistep creep results do not fall on this master curve, particularly for step B. The labels A−D refer to Figure 5, and the arrows indicate the direction of time. (b) Strain rate as a function of mobility for the multistep creep simulation shown in Figure 8. The "×" points are from single-step creep deformations (Figure 6 and ref 38). The single-step data from the simulation also show a good correlation between mobility and strain rate, except for the first measurement after applying the stress ("◐" points). The dashed line is a guide to the eye. The multistep creep deformations show a different relationship between strain rate and mobility, most notably in step B. The labels A−D refer to Figure 8.

simulation temperature, although low by simulation standards, is not low enough to produce dynamics as slow as those observed in experiments on polymeric glasses. If only experiments had been performed, then it could be argued that the motion of the probe molecules may not reflect the motion of the surrounding polymer chains. Given that the simulations and experiments show remarkably similar behavior, the simplest interpretation of the combined results is that the simulation model is adequate, the simulation time scales are long enough, and the probes are faithful reporters of the polymer segmental dynamics.

The combination of experiment and simulation allows us to address a fundamental issue about the interpretation of the experimental results. We interpret faster anisotropy decay functions as enhanced segmental mobility and, in so doing, make an analogy to the mobility that occurs when a glass is heated to a higher temperature. Others might view the experiments as merely showing that deforming polymer glasses causes the polymer segments and probes to rearrange in the same way that twisting a handle might cause gears to turn. In this latter view, the term "mobility" has no place in the interpretation of the experimental results. The simulations provide important insight into this issue. In previous work,[21] it was shown that several different measures of polymer mobility (bond reorientation and the decay of dynamic incoherent structure factor at multiple wave vectors and multiple directions) accelerate by the same amount during uniaxial deformation. This result is consistent with the interpretation that deformation produces mobility and not just rearrangement. Given the similarity between the experiments and simulations, it is also reasonable to interpret the experiments in terms of enhanced segmental mobility.

Conclusions

Using an optical experimental method and MD simulations, we have measured segmental mobility in polymer glasses during tensile creep deformation. Our results indicate that a strong correlation between strain rate and mobility exists in single-step creep. However, in multistep creep and recovery, the correlation between strain rate and mobility is broken in both experiment and simulation. This is consistent with the view that no simple mechanical variable universally exhibits a simple relationship with molecular mobility. The lower mobility observed immediately after the stress is reapplied in both multistep experiments and simulations is consistent with the "stress aging" phenomenon reported by Kramer. In contradiction to the Eyring model, we observe an increase in segmental mobility immediately following a significant drop in stress in both experiments and simulations and a wide range of mobilities (up to a factor of 100) during constant true stress. In addition, an increase in the KWW β parameter after flow onset in the experiments indicates that spatially heterogeneous dynamics plays a significant role in the deformation mechanism of polymer glasses. A molecular interpretation of deformation-induced transition from a low-mobility glass to a homogeneous and mobile material will be explored in a future publication.[31]

Acknowledgment. This work was supported by the National Science Foundation (NIRT 0506840, DMR-0520527, and DMR-0907607). We thank Jim Caruthers, Ed Kramer, and Ken Schweizer for useful discussions. We thank Lian Yu and Ye Sun for performing DSC measurements.

References and Notes

(1) Meijer, H. E. H.; Govaert, L. E. *Prog. Polym. Sci.* **2005**, *30*, 915–938.
(2) Haward, R. N.; Thackray, G. *Proc. R. Soc. London, Ser. A* **1968**, *302*, 453.
(3) Buckley, C. P.; Jones, D. C. *Polymer* **1995**, *36*, 3301–3312.
(4) Boyce, M. C.; Parks, D. M.; Argon, A. S. *Mech. Mater.* **1988**, *7*, 15–33.
(5) Schapery, R. A. *Int. J. of Solids Struct.* **1966**, *2*, 407–425.
(6) Schapery, R. A. *Polym. Eng. Sci.* **1969**, *9*, 295–310.
(7) Popelar, C. F.; Liechti, K. M. *J. Eng. Mater. Technol.* **1997**, *119*, 205–210.
(8) Popelar, C. F.; Liechti, K. M. *Mech. Time-Depend. Mater.* **2003**, *7*, 89–141.
(9) Shay, R. M.; Caruthers, J. M. *Polym. Eng. Sci.* **1990**, *30*, 1266–1280.
(10) Lustig, S. R.; Shay, R. M.; Caruthers, J. M. *J. Rheol.* **1996**, *40*, 69–106.
(11) Caruthers, J. M.; Adolf, D. B.; Chambers, R. S.; Shrikhande, P. *Polymer* **2004**, *45*, 4577–4597.
(12) Eyring, H. *J. Chem. Phys.* **1936**, *4*, 283.
(13) Argon, A. S. *Philos. Mag.* **1973**, *28*, 839–865.
(14) Chen, K.; Schweizer, K. S. *Europhys. Lett.* **2007**, *79*, 26006.
(15) Robertson, R. E. *J. Chem. Phys.* **1966**, *44*, 3950.
(16) Boeing: Commercial Airplanes: 787 Dreamliner Program Fact Sheet.http://www.boeing.com/commercial/787family/program-facts.html.
(17) Lee, H.-N.; Paeng, K.; Swallen, S. F.; Ediger, M. D. *J. Chem. Phys.* **2008**, *128*, 134902.
(18) Lee, H.-N.; Paeng, K.; Swallen, S. F.; Ediger, M. D. *Science* **2009**, *323*, 231–234.
(19) Lee, H.-N.; Paeng, K.; Swallen, S. F.; Ediger, M. D.; Stamm, R. A.; Medvedev, G. A.; Caruthers, J. M. *J. Polym. Sci., Part B: Polym. Phys.*, submitted.

(20) Riggleman, R. A.; Lee, H.-N.; Ediger, M. D.; de Pablo, J. J. *Phys. Rev. Lett*. **2007**, *99*, 215501.
(21) Riggleman, R. A.; Schweizer, K. S.; de Pablo, J. J. *Macromolecules* **2008**, *41*, 4969–4977.
(22) Chen, K.; Schweizer, K. S. *Macromolecules* **2008**, *41*, 5908–5918.
(23) Martinez-Vega, J. J.; Trumel, H.; Gacougnolle, J. L. *Polymer* **2002**, *43*, 4979–4987.
(24) Loo, L. S.; Cohen, R. E.; Gleason, K. K. *Science* **2000**, *288*, 116–119.
(25) Zhou, Q. Y.; Argon, A. S.; Cohen, R. E. *Polymer* **2001**, *42*, 613–621.
(26) Capaldi, F. M.; Boyce, M. C.; Rutledge, G. C. *Phys. Rev. Lett*. **2002**, *89*, 175505.
(27) Capaldi, F. M.; Boyce, M. C.; Rutledge, G. C. *Polymer* **2004**, *45*, 1391–1399.
(28) Lyulin, A. V.; Balabaev, N. K.; Mazo, M. A.; Michels, M. A. J. *Macromolecules* **2004**, *37*, 8785–8793.
(29) Lyulin, A. V.; Vorselaars, B.; Mazo, M. A.; Balabaev, N. K.; Michels, M. A. J. *Europhys. Lett*. **2005**, *71*, 618–624.
(30) Warren, M.; Rottler, J. *Phys. Rev. E* **2007**, *76*, 031802.
(31) Riggleman, R. A.; Lee, H.-N.; Ediger, M. D.; de Pablo, J. J. *Soft Matter*, submitted.
(32) Cicerone, M. T.; Ediger, M. D. *J. Phys. Chem*. **1993**, *97*, 10489–10497.
(33) Papakonstantopoulos, G. J.; Riggleman, R. A.; Barrat, J.-L.; de Pablo, J. J. *Phys. Rev. E* **2008**, *77*, 041502.
(34) Tzoumanekas, C.; Theodorou, D. N. *Macromolecules* **2006**, *39*, 4592–4604.
(35) Banaszak, B. J.; de Pablo, J. J. *J. Chem. Phys*. **2003**, *119*, 2456–2462.
(36) Bennemann, C.; Paul, W.; Baschnagel, J.; Binder, K. *J. Phys.: Condens. Matter* **1999**, *11*, 2179–2192.
(37) Kramer, E. J. *J. Appl. Phys*. **1970**, *41*, 4327.
(38) Riggleman, R. A.; Toepperwein, G. N.; Papakonstantopoulos, G. J.; de Pablo, J. J., *Macromolecules* **2009**, *42*, 3632−3640.
(39) Ediger, M. D. *Annu. Rev. Phys. Chem*. **2000**, *51*, 99–128.
(40) Park, J.-W.; Ediger, M. D.; Green, M. M. *J. Am. Chem. Soc*. **2001**, *123*, 49–56.
(41) Thurau, C. T.; Ediger, M. D. *J. Chem. Phys*. **2002**, *116*, 9089–9099.
(42) Chen, K.; Schweizer, K. S. *Phys. Rev. Lett*. **2009**, *102*, 4.
(43) Lyulin, A. V.; Michels, M. A. J. *Phys. Rev. Lett*. **2007**, *99*, 085504.
(44) Lacks, D. J.; Osborne, M. J. *Phys. Rev. Lett*. **2004**, *93*, 255501.